(Received 17 April 2026, Accepted 18 May 2026, Scheduled 5 June 2026)

A Compact Four-Port Circularly Polarized MIMO Antenna Using a Polarization Conversion Superstrate

Jingchang Nan, Siyao Zhao*, and Yifei Wang

School of Electronic and Information Engineering, Liaoning Technical University, Huludao 125105, China

ABSTRACT: A compact four-port circularly polarized multiple-input multiple-output (CP-MIMO) antenna with a dual-layer architecture is proposed for low-altitude communication. In compact MIMO arrays of CP-capable monopole elements, strong mutual coupling makes stable CP radiation difficult to achieve. To address this issue, the proposed antenna uses a lower layer for dual-polarized MIMO generation and an upper layer for polarization conversion. The antenna was fabricated on two FR-4 substrates with an overall size of $0.85\lambda \times 0.85\lambda \times 0.084\lambda$. In the lower layer, a dual-polarized feed backplane (DPFB) forms a $\pm 45^{\circ}$ dual-polarized MIMO array with port isolation exceeding 17 dB. In the upper layer, a polarization conversion superstrate (PCS) converts the incident dual-polarized waves into CP radiation. The PCS extended the impedance bandwidth by 36%, from 7.55 to 10.08 GHz, and enabled LHCP radiation with a 3 dB axial ratio bandwidth of 8.22–8.89 GHz. A gain enhancement of 48% was also achieved. The measured results verified the design and demonstrated good MIMO diversity performance.

1. INTRODUCTION

The rapid development of the low-altitude economy has led to a growing demand for advanced wireless communication systems [1–3]. Emerging applications, such as unmanned aerial vehicle (UAV) swarms, urban air mobility (UAM), and low-altitude logistics, require compact, lightweight, and highly integrated antenna systems [4]. These systems must support high data rates, strong interference suppression, and reliable link performance under strict size and platform constraints [5, 6]. In addition, the dynamic operating environments of such platforms, including frequent movement and orientation variations, impose stringent requirements on antenna stability and robustness [7, 8].

Multiple-input multiple-output (MIMO) technology has been widely adopted to improve channel capacity and spectral efficiency by exploiting spatial diversity [9–11]. By utilizing multiple antennas, MIMO systems can effectively mitigate fading effects and enhance the signal reliability in complex propagation environments. Meanwhile, circular polarization (CP) provides additional advantages, such as reduced sensitivity to antenna misalignment and improved immunity to multipath interference [12, 13]. Therefore, combining MIMO with CP has become an effective solution for improving both the link reliability and transmission efficiency. Consequently, CP-MIMO antennas have attracted significant attention in recent years, particularly for compact wireless platforms in low-altitude communication systems [14–16].

Various techniques have been proposed for integrating CP functionality into MIMO systems. A commonly used approach is to realize circular polarization directly at the antenna element level and then arrange these elements into a MIMO array. Typical designs employ meandered lines [17], slot-loaded patches [18, 19], or parasitic elements [20] to excite two orthogonal modes with a 90° phase difference. However, in such configurations, the CP performance is strongly dependent on the geometry of individual elements. When these CP-capable elements are placed in close proximity to form a compact MIMO array, strong mutual coupling occurs inevitably. This coupling disturbs the current distribution on the radiating elements and leads to a significant degradation of the axial ratio (AR). Consequently, stable CP radiation can only be achieved through careful and often iterative optimization, involving tradeoffs among the AR, port isolation, and impedance matching. This process not only increases the design complexity but also limits the flexibility of the overall antenna design.

Another approach introduces CP through feeding networks or auxiliary structures before forming a MIMO array. For instance, orthogonal slot-coupled feeding combined with a polarization conversion metasurface was reported in [21]. Unequal-length feeding of dielectric resonator antennas (DRAs) has also been utilized to generate the required phase difference [22]. Although these methods can effectively produce circular polarization, they often suffer from a relatively large physical size or limited bandwidth. In particular, DRAs are not well suited for compact X-band applications, where a low profile and wide impedance bandwidth are required simultaneously.

Despite these research efforts, achieving stable CP radiation in compact MIMO arrays remains challenging. The main difficulty lies in the strong mutual coupling between closely spaced elements, which makes it difficult to maintain both stable polarization characteristics and good MIMO performance. More importantly, it is still difficult to achieve stable CP radiation

* Corresponding author: Siya Zhao (13842387706@163.com).

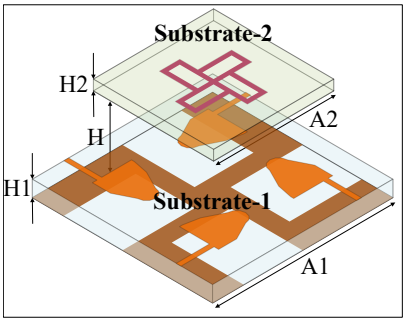

FIGURE 1. Exploded three-dimensional view of the proposed CP-MIMO antenna.

without modifying the original array structure or degrading its inherent impedance matching and isolation properties.

To address this challenge, this study proposes a compact four-port CP-MIMO antenna based on a dual-layer architecture. In the lower layer, a dual-polarized feed backplane (DPFB) is employed to reconfigure four umbrella-shaped monopoles into a $\pm 45^{\circ}$ dual-polarized MIMO array with improved port isolation. This configuration provides a balanced amplitude and consistent phase excitation, which are essential for polarization control. In the upper layer, a polarization conversion superstrate (PCS) is introduced as an independent, transmissive phase-control structure. By manipulating the phases of the incident orthogonal components, the PCS converts dual-polarized waves into circularly polarized radiation.

With this decoupled configuration, the proposed design separates the MIMO generation and polarization conversion into two coordinated functional layers. The proposed dual-layer design separates MIMO generation and polarization conversion. This avoids the difficulty of simultaneously handling both functions in a single layer and enables step-by-step design of impedance matching, isolation, and polarization characteristics. Consequently, stable CP radiation is achieved without modifying the original array structure, while the inherent MIMO performance of the lower layer is preserved. This design strategy provides a flexible and efficient solution for compact CP-MIMO antennas with a low profile.

2. CP-MIMO ANTENNA DESIGN

The proposed CP-MIMO antenna was developed using a three-stage design strategy, in which the radiation and polarization characteristics were progressively established. In the first stage, a CP-capable monopole element was designed as the fundamental radiating unit, providing the basis for broadband impedance matching and initial polarization control through structural asymmetry. In the second stage, a dual-polarized feed backplane (DPFB) is introduced to reconfigure four monopole elements into a compact MIMO array with $\pm 45^{\circ}$ dual-polarized radiation. This configuration not only improves port isolation but also generates two orthogonal linear polarization (LP) components with balanced amplitude and stable phase characteristics, which are essential for circular polarization (CP) formation. In the third stage, a polarization conversion superstrate (PCS) is deployed above the MIMO array as an independent transmissive phase-control structure to convert the incident dual-polarized waves into circularly polarized radiation.

The exploded three-dimensional view of the proposed antenna is illustrated in Fig. 1, which clearly shows the layered configuration of the structure. The detailed geometries of the MIMO array, DPFB, and integrated antenna are shown in Fig. 2, and the corresponding geometric parameters are summarized in Table 1.

TABLE 1. Antenna geometrical parameters (unit: mm).

Parameter	H	H1	H2	A1	A2	R	WH
Dimension	2.3	0.7	0.25	30	20	3	6
Parameter	WF	LS	WS	HP	WP	LP	
Dimension	5.5	3	5.2	0.75	3.375	12	

2.1. CP Monopole Antenna Design

Figure 3 shows the geometry of the proposed monopole antenna element. The antenna was printed on an FR-4 substrate with dimensions of $0.43\lambda \times 0.43\lambda \times 0.02\lambda$ and is fed by a microstrip line. Based on the method reported in [19], circularly polarized (CP) radiation can be achieved by introducing geometric asymmetry to perturb the surface current distribution on the radiating element. Accordingly, an asymmetric umbrella-shaped geometry was adopted in this study.

The corresponding simulated performance of the antenna element is presented in Fig. 4, where Fig. 4(a) and Fig. 4(b) show the reflection coefficient (S_{11}) and axial ratio (AR), respectively. As shown in Fig. 4(b), the initial symmetrical configuration (Ant. 1) exhibits only linear polarization (LP) owing to the absence of asymmetrical perturbation. As the geometry evolves from Ant. 1 through the intermediate configurations to Ant. proposed, impedance matching is well maintained while the axial ratio is progressively improved. This indicates that the introduced asymmetry effectively modifies the current distribution and excites two orthogonal modes with an appropriate phase difference, thereby enabling CP radiation. The final antenna element (Ant. proposed) achieves an impedance bandwidth of 8.22–11.87 GHz and a 3 dB AR bandwidth of 8.11–10.4 GHz, indicating favorable broadband CP performance.

2.2. Dual-Polarized MIMO Array and DPFB Design

Based on the proposed umbrella-shaped monopole element, a compact dual-polarized MIMO array was constructed on an FR-4 substrate with overall dimensions of $0.85\lambda \times 0.85\lambda \times 0.02\lambda$. As illustrated in Fig. 2(a), the four umbrella-shaped monopoles are orthogonally arranged at 0°, 90°, 180°, and 270°, forming a rotationally symmetric layout that effectively exploits both spatial diversity and polarization diversity. This configuration not only supports multi-port operation but also establishes the necessary conditions for generating orthogonal polarization states in subsequent designs.

However, when a conventional backplane structure is implemented, strong electromagnetic coupling arises among closely spaced elements owing to overlapping near-field distributions and shared current paths on the ground plane. Consequently,

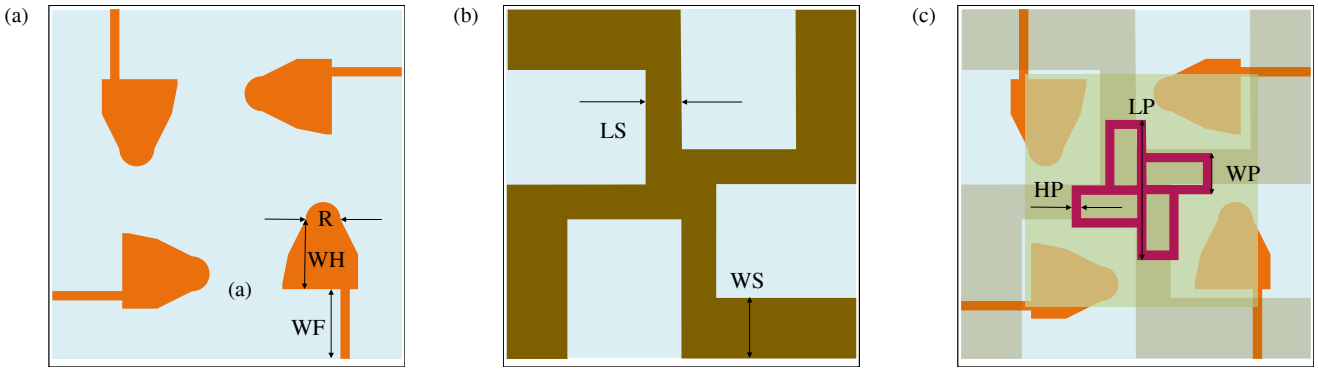

FIGURE 2. Geometry of the proposed CP-MIMO antenna: (a) top view of the MIMO array, (b) dual-polarized feed backplane (DPFB), and (c) top view of the integrated antenna.

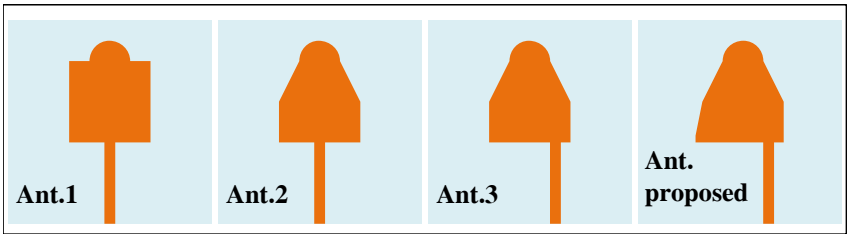

FIGURE 3. Geometry evolution of the proposed monopole antenna element.

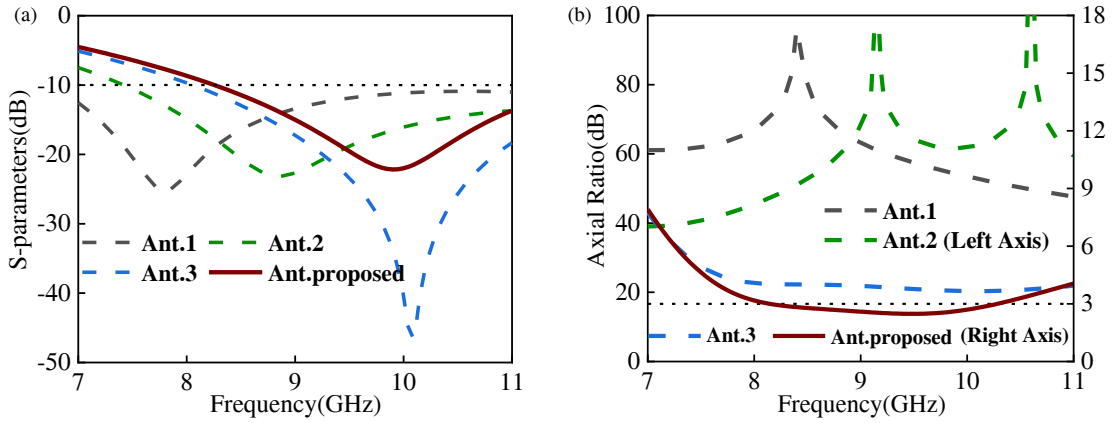

FIGURE 4. Simulated performance of the antenna element: (a) reflection coefficient (S_{11}) and (b) axial ratio.

the port isolation of the MIMO array was limited to approximately 15 dB. Such isolation is insufficient for practical MIMO systems, where high isolation is essential to suppress the mutual coupling, preserve the channel independence, and maintain stable radiation characteristics. Therefore, further modifications of the feeding and grounding structures are required to enhance the isolation performance while retaining the compact array configuration.

To enhance port isolation, a dual-polarized feed backplane (DPFB) based on a shared ground-plane configuration [17] is introduced. Although the proposed structure is geometrically similar to that in [17], the feed parameters are re-optimized to accommodate the present four-port MIMO array configuration. The DPFB effectively redistributes the surface current paths, thereby improving inter-port isolation without increasing the structural complexity.

With the incorporation of the DPFB, the array maintains good impedance matching over 7.99–9.85 GHz (Fig. 5(a)). Meanwhile, the adjacent-port isolation exceeded 17 dB, and the diagonal-port isolation was better than 26 dB (Fig. 5(b)), demonstrating the effectiveness of the DPFB in mitigating mutual coupling in a compact layout.

Based on the shared-ground structure in [17], the modified DPFB was demonstrated to generate dual-polarized excitation, which was not reported in [17]. Beyond isolation improvement, the DPFB also plays a critical role in establishing stable dual-polarized radiation. Specifically, it introduces two orthogonal current modes along the $\pm 45^{\circ}$ directions. According

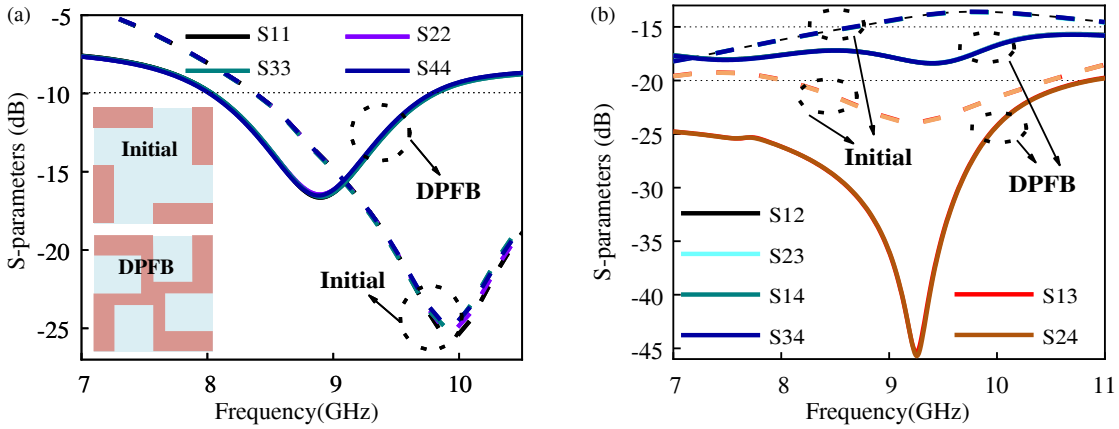

FIGURE 5. Performance of the dual-polarized MIMO array and DPFB: (a) Geometry of the DPFB and reflection coefficients. (b) Isolation characteristics.

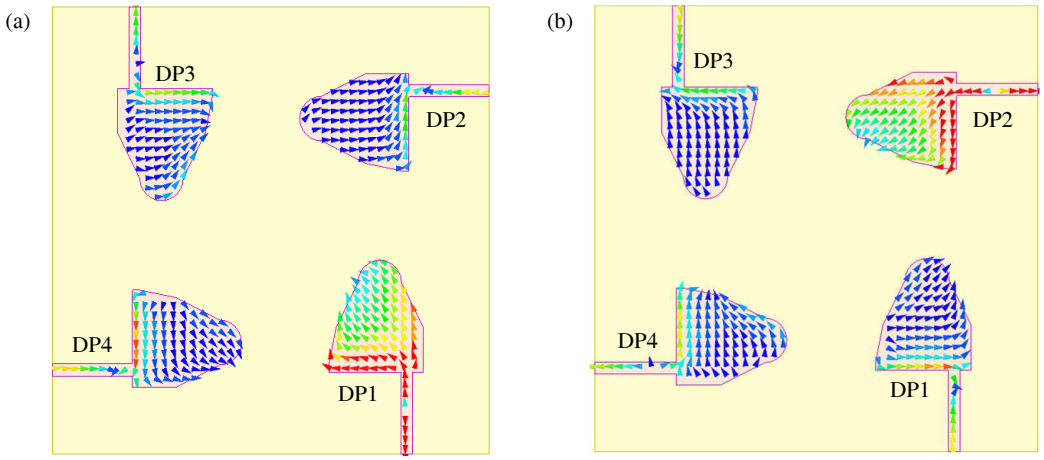

FIGURE 6. Surface current distributions of the dual-polarized MIMO array: (a) DP1 excited; (b) DP2 excited.

to the surface-current-based polarization verification method in [23], when only DP1 is excited (Fig. 6(a)), the dominant current flows along the $-45°$ direction, whereas the excitation of DP2 (Fig. 6(b)) results in a current flowing along the $+45°$ direction. This orthogonal current distribution directly leads to the generation of $\pm 45°$ linear polarizations.

Furthermore, owing to the $180°$ rotational symmetry of the array, DP3 and DP4 can be regarded as rotated counterparts of DP1 and DP2, respectively, ensuring consistent electromagnetic behavior across all ports. As a result, DP1 and DP3 produced $-45°$ linear polarization (LP), whereas DP2 and DP4 generated $+45°$ LP, forming two orthogonal polarization pairs with balanced amplitude characteristics. The well-aligned S_{11}−-S_{44} responses further confirm the uniform impedance performance among all ports.

In summary, the DPFB-based MIMO configuration not only enhances port isolation by suppressing the coupling paths, but also enables the formation of stable and orthogonal $\pm 45°$ LP modes. These features provide well-defined and balanced incident fields that are essential for the subsequent polarization conversion stage.

2.3. Integrated CP-MIMO Antenna with PCS

Although the DPFB provides stable dual-polarized excitation, the MIMO array alone is still incapable of generating circularly polarized (CP) radiation. This limitation is clearly evidenced by the axial ratio (AR), which remains above 10 dB across the operating band, as shown in Fig. 7(c). This indicates that the two orthogonal linear polarization components lack the required quadrature phase relationship for CP formation.

To overcome this limitation, a polarization conversion surface (PCS) was introduced above the array as an independent transmissive phase-control layer. By leveraging the wavefront manipulation mechanism of metasurfaces [24], the PCS modifies the phase response of the incident orthogonal components, thereby introducing an additional $90°$ phase difference. Consequently, the incident $\pm 45°$ linearly polarized waves were converted into circularly polarized radiation.

The PCS was fabricated on an FR-4 substrate with a thickness of 0.007λ and overall dimensions of $0.57\lambda \times 0.57\lambda$. It is separated from the lower-layer array by an air gap of height H, which provides sufficient space for effective electromagnetic coupling and phase accumulation to occur. As illustrated in Fig. 2(c), the PCS consists of a periodic windmill-shaped

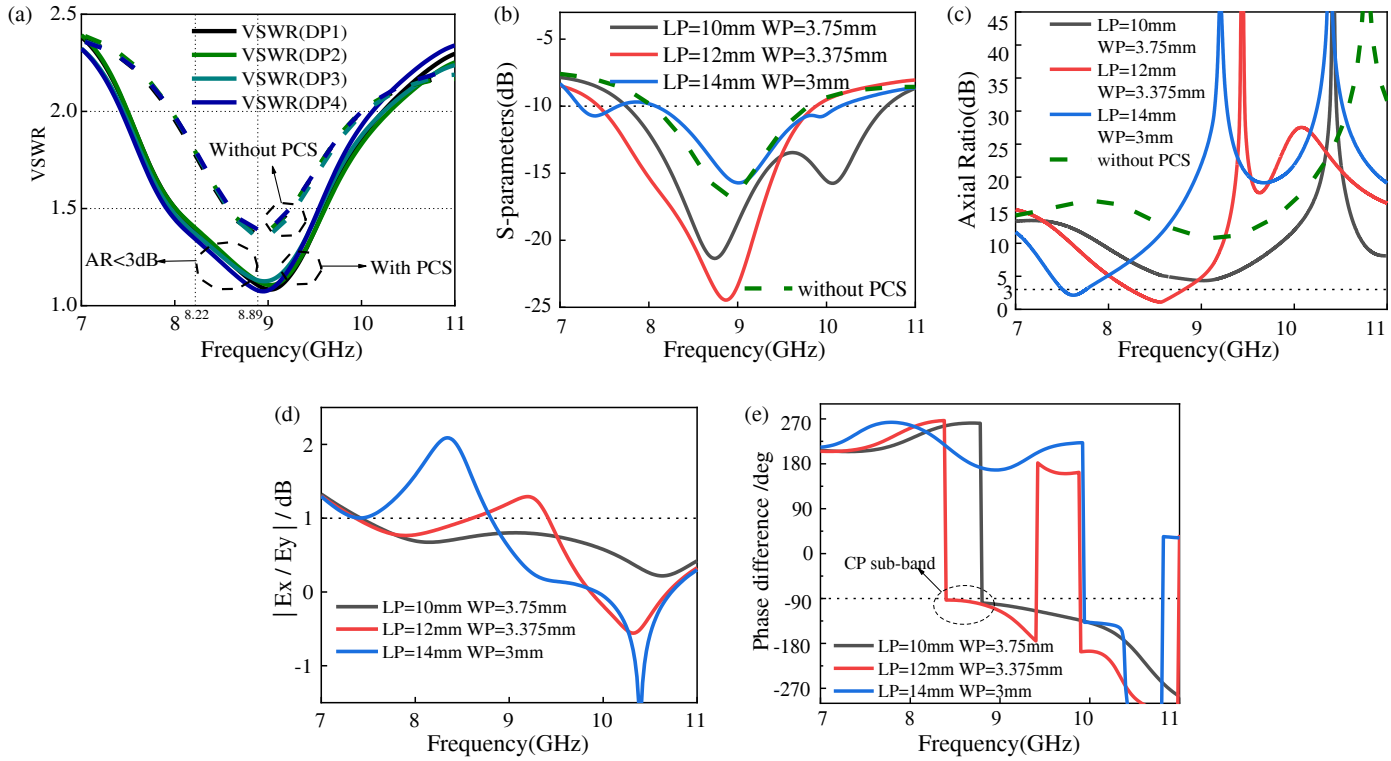

FIGURE 7. (a) Simulated four-port VSWR w/o PCS. (b) Return loss for different (Lp, Wp), compared w/o PCS. (c) AR for different (Lp, Wp), compared w/o PCS. (d) Amplitude ratio (|Ex/Ey|), and (e) phase difference.

slot structure formed by four identical rectangular slots rotated by 90° with respect to each other. Each slot has dimensions of $L_p/2$ and W_p, and the spacing between adjacent slots is denoted as H_p. This geometrical arrangement enables anisotropic phase responses along orthogonal directions, satisfying the wavefront manipulation condition reported in [25].

The polarization conversion mechanism of the PCS can be explained as follows. The incident ±45° dual-polarized waves were first decomposed into two orthogonal linear components along the 0° and 90° directions. These two components have equal amplitudes but different orientations, forming the basis for subsequent phase manipulation.

Owing to the rotational symmetry of the windmill-shaped slot, the two orthogonal components interact selectively with different parts of the PCS. Specifically, the 0° component mainly couples to the horizontal rectangular sections, whereas the 90° component predominantly interacts with the vertical rectangular sections. This directional selectivity ensures that the two orthogonal components follow distinct transmission paths in the PCS.

Because these transmission paths are geometrically different, the corresponding electromagnetic responses are also different, resulting in a phase difference $\Delta\varphi$ between the transmitted fields. By properly optimizing the geometrical parameters of the PCS, this phase difference can be tuned to approach 90° within the target frequency range. When combined with the equal-amplitude condition, this phase relationship enables the formation of circularly polarized radiation.

To optimize the PCS dimensions, the voltage standing wave ratio (VSWR) and axial ratio (AR) were analyzed. As shown in Fig. 7(a), the VSWR of all four ports remains below 2 over 7.55–10.08 GHz, and is further reduced to below 1.5 within the CP operating band of 8.22–8.89 GHz. Compared with the case without the PCS, the impedance bandwidth is extended from 7.99–9.85 GHz to 7.55–10.08 GHz, corresponding to an increase in the relative bandwidth from 20.9% to 28.7% (a 36% enhancement). These results indicate that the introduction of the PCS does not degrade the impedance matching performance, but instead contributes to bandwidth improvement.

Figures 7(b) and 7(c) further illustrate the effects of different L_p and W_p combinations on the impedance matching and AR performance. Fig. 7(d) and Fig. 7(e) show the corresponding amplitude ratio ($|E_x/E_y|$) and phase difference between the orthogonal components under different PCS dimensions. It can be observed that modifying the slot length and width effectively tunes both the amplitude ratio and phase response of the orthogonal components. In particular, within the target CP band, the amplitude ratio remains close to 1 while the phase difference approaches 90°, satisfying the circular polarization condition. These results further verify that the windmill-shaped PCS provides controllable orthogonal phase manipulation through the rectangular slot geometry. Consequently, a 3 dB AR bandwidth of 8.22–8.89 GHz was achieved. In addition, the PCS enhances the realized gain within the CP band through near-field coupling between the PCS and radiating elements. As shown in Fig. 9(b), the realized gain increases from 0.71–1.53 dBi to

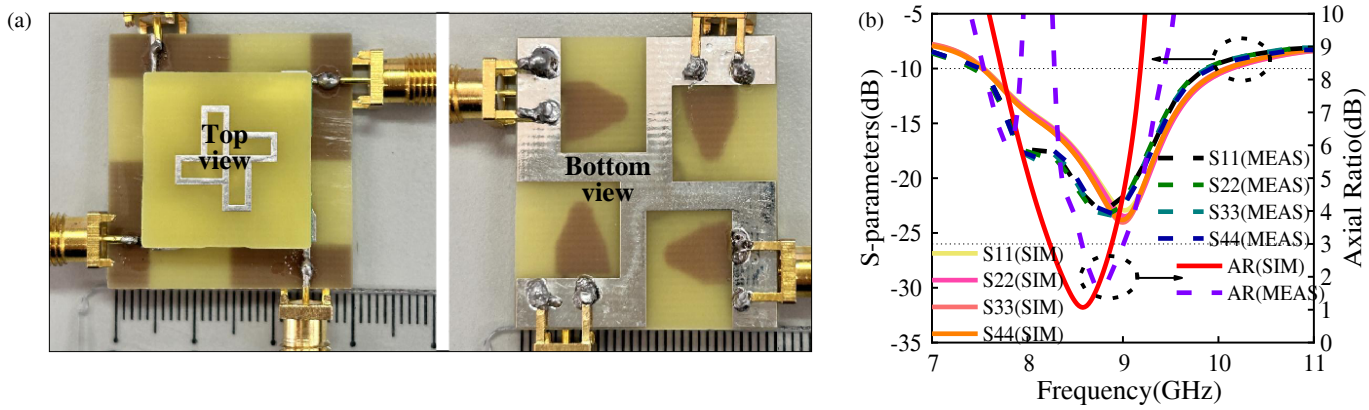

FIGURE 8. Fabricated antenna prototype and measured results: (a) top and bottom views, and (b) measured return loss and axial ratio.

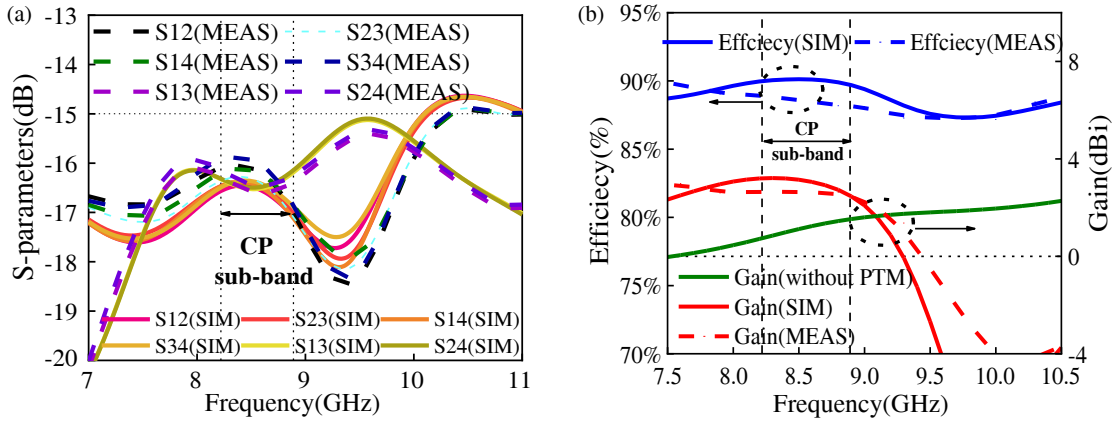

FIGURE 9. Measured performance of the proposed antenna: (a) transmission coefficient (dB), and (b) gain (dBi) and radiation efficiency.

2.46–3.21 dBi, indicating a significant improvement in the radiation performance.

In summary, the PCS functions as an independent transmissive phase-control layer that converts incident dual-polarized waves into circularly polarized radiation without modifying the underlying MIMO array structure. Meanwhile, through the combined effects of phase regulation and near-field coupling, it also improves the impedance bandwidth and enhances the realized gain of the antenna system.

3. SIMULATED AND MEASURED RESULTS

Figure 8(a) shows the fabricated dual-layer antenna prototype, which includes the lower MIMO array and upper PCS layer. In the fabricated prototype, the air gap between the two substrates is practically supported by a PTFE spacer ring with a relative permittivity of 2.1 and a loss tangent of 0.0002. The spacer has an inner diameter of 3 mm, outer diameter of 6 mm, and thickness of 2.3 mm, and is placed at the center between the two layers. To evaluate the possible influence of fabrication support structures, the PTFE spacer was also included in the HFSS model during simulation. The results show only minor differences compared with the ideal air-gap case, confirming that the practical support structure introduces negligible effects on the antenna performance. Minor discrepancies between the simulated and measured results are mainly attributed to practical fabrication and assembly factors, including fabrication tolerances, layer alignment deviations, and SMA connector soldering effects.

The S-parameters were measured using a vector network analyzer (VNA). As shown in Fig. 8(b), the measured results indicate a -10 dB impedance bandwidth of 7.49–9.87 GHz. Within this band, a 3 dB axial ratio (AR) bandwidth of 8.56–9.01 GHz was achieved, confirming effective circular polarization generation in the target frequency range.

Meanwhile, the measured isolation (Fig. 9(a)) is better than 15.9 dB across the operating band, demonstrating that the DPFB-based structure maintains good decoupling performance even after integrating the PCS layer. Compared with the simulated lower MIMO array without the PCS in Fig. 5(b), the isolation slightly decreases because the PCS introduces additional electromagnetic coupling paths between the ports. Nevertheless, the measured isolation still satisfies practical MIMO requirements. Overall, the measured results were in good agreement with the simulations, validating the effectiveness and reliability of the proposed design.

The radiation characteristics were measured in a standard anechoic chamber. As shown in Fig. 9(b), within the measured CP band, the realized gain ranged from 1.42 to 2.78 dBi, whereas the radiation efficiency remained higher than 89.3%.

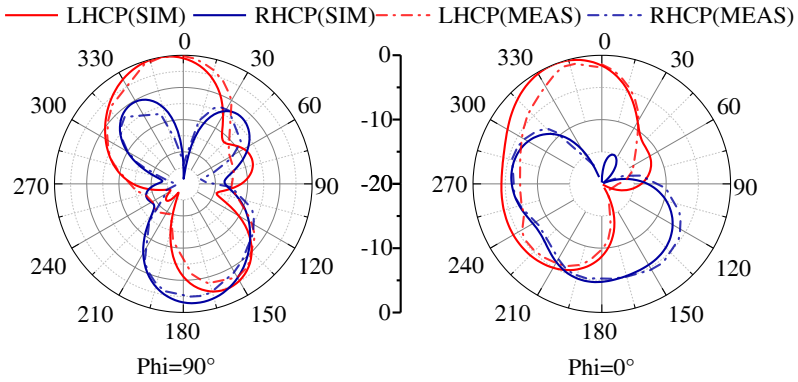

FIGURE 10. Simulated and measured LHCP and RHCP radiation patterns at $\varphi = 0°$ and $\varphi = 90°$.

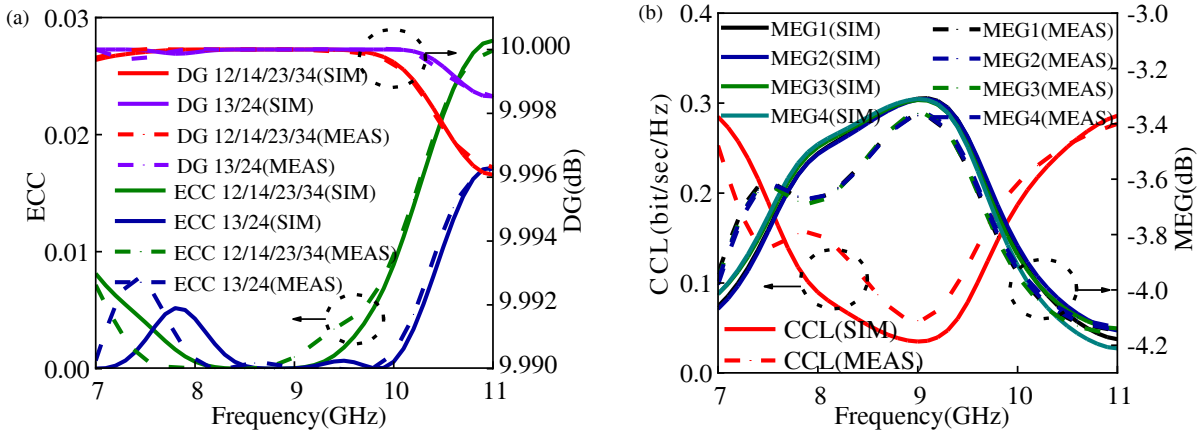

FIGURE 11. Simulated and measured results: (a) ECC and DG (dB), and (b) CCL and MEG.

Owing to the dual-layer air-gap configuration and transmissive PCS structure, the electromagnetic field is not strongly confined inside the FR-4 substrate, which helps maintain relatively high radiation efficiency despite operation at X-band. The results indicate that the introduction of the PCS not only enables polarization conversion but also maintains a high radiation efficiency and stable gain performance.

Figure 10 compares the simulated and measured LHCP and RHCP radiation patterns at $\phi = 0°$ and $\phi = 90°$. Good agreement between the simulation and measurement was observed, with only minor discrepancies. Compared with the broad forward beam of the lower-layer MIMO antenna without the PCS, the integrated dual-layer CP-MIMO antenna exhibits a more concentrated forward main beam after introducing the PCS, while no obvious back-lobe enhancement is observed. This indicates that the PCS mainly performs transmissive phase control and polarization conversion without degrading the radiation pattern. The enhanced forward directivity is also consistent with the measured gain improvement and radiation efficiency higher than 89.3%. Simulated and measured differences can be attributed to fabrication tolerances and measurement uncertainties. The antenna exhibits high polarization purity, and the LHCP/RHCP discrimination in the main beam exceeds 18 dB, confirming effective circular polarization with low cross-polarization levels.

The MIMO diversity performance of the proposed antenna was also evaluated. As shown in Fig. 11(a), the envelope correlation coefficient (ECC) remains below 0.01, indicating very low channel correlation between antenna ports, while the diversity gain (DG) is higher than 9.99 dB, approaching the ideal diversity performance. Furthermore, Fig. 11(b) shows that the channel capacity loss (CCL) is below 0.156 bps/Hz, and the mean effective gain (MEG) is lower than -3.36 dB across the operating band, satisfying the commonly accepted criteria for practical MIMO systems. These results confirm that the proposed antenna not only achieves stable circular polarization performance, but also maintains satisfactory diversity and multi-port MIMO characteristics for practical communication applications [20, 26].

4. COMPARISON

Table 2 compares the proposed antenna with previously reported CP-MIMO designs in terms of key performance metrics, including the impedance bandwidth, axial ratio (AR) bandwidth, gain, and structural compactness. It can be clearly observed that the proposed antenna achieves the widest impedance bandwidth of 28.7% among the compared designs, while maintaining a compact four-port configuration with an overall size of $0.85\lambda \times 0.85\lambda \times 0.084\lambda$. This demonstrates its

TABLE 2. Comparison of CP-MIMO antennas.

Ref.	Impedance bandwidth (%)	AR bandwidth (%)	Size ($\lambda \times \lambda \times \lambda$)	Ports	ΔGain (%)
[18]	23.3	1.28/3.17	$2.9 \times 1.8 \times 0.04$	2	-
[27]	9.3	9.3	$1.36 \times 0.94 \times 0.05$	2	-
[28]	3.2	6.2	$1.25 \times 0.83 \times 0.01$	2	35.2
[29]	9/105.9	4.3/67.7	$1.98 \times 1.93 \times 0.045$	4	-
[30]	7.05	2.04	$1.4 \times 1.4 \times 0.03$	4	12.5
This work	28.7	7.83	$0.85 \times 0.85 \times 0.084$	4	48

capability to provide wideband operation without sacrificing structural compactness.

In addition, a 3 dB AR bandwidth of 7.83% was obtained, indicating stable circularly polarized performance over the operating band. The realized gain was also significantly improved, with an enhancement of 48% compared to the reference configuration without the polarization conversion layer. These results confirm that the proposed antenna achieves a wide impedance bandwidth while maintaining satisfactory polarization purity and radiation efficiency.

It is worth emphasizing that, unlike conventional CP-MIMO designs, where circular polarization is directly generated within the antenna elements, the proposed antenna adopts a decoupled design strategy by separating dual-polarized MIMO formation and CP generation into two coordinated functional layers. This configuration allows the impedance matching, port isolation, and polarization characteristics to be optimized independently, thereby reducing the design complexity and improving the performance stability.

The proposed antenna achieves a favorable balance among compact size, number of ports, impedance bandwidth, and radiation performance. Compared with existing designs, it provides a more flexible and effective solution for realizing high-performance CP-MIMO antennas on compact and integrated platforms.

5. CONCLUSION

This study presents a compact four-port circularly polarized multiple-input multiple-output (CP-MIMO) antenna for low-altitude communication applications. Stable circular polarization is achieved without modifying the underlying array structure by introducing an upper-layer polarization conversion superstrate above a dual-polarized MIMO array structure. This dual-layer configuration separates the MIMO generation and polarization conversion, thereby enabling effective and flexible performance optimization. The measured results verify the effectiveness of the proposed design, demonstrating an extended impedance bandwidth, enhanced gain, stable LHCP radiation, and satisfactory MIMO diversity performance. These results indicate that the antenna achieves a good balance between wideband operation, polarization purity, and multi-port characteristics. Owing to its compact size and favorable radiation properties, the proposed antenna is well-suited for space-constrained low-altitude platforms, such as UAV terminals and low-altitude IoT nodes. Furthermore, due to the functional separation between the lower MIMO radiating layer and the upper PCS layer, the proposed dual-layer architecture also provides good scalability for higher-order CP-MIMO array designs.

ACKNOWLEDGEMENT

This work was supported by the National Natural Science Foundation of China under Grant No. 61971210.

REFERENCES

[1] Cheng, T., J. Tang, S. Li, C. Yang, Y. Xiang, and X. Song, "Communications for low-altitude economy: A precoding transmission method for RIS-assisted UAV communication," in *2025 6th International Symposium on Computer Engineering and Intelligent Communications (ISCEIC)*, 7–12, Chongqing, China, Nov. 2025.

[2] Huang, H., J. Su, and F.-Y. Wang, "The potential of low-altitude airspace: The future of urban air transportation," *IEEE Transactions on Intelligent Vehicles*, Vol. 9, No. 8, 5250–5254, Aug. 2024.

[3] Feng, L., H. Liu, Y. Zhao, X. Wang, F. Zhou, and W. Li, "Semantic communication for low-altitude economy: Harnessing the power of generative AI and edge intelligence," *IEEE Wireless Communications*, Vol. 33, No. 1, 36–44, 2026.

[4] Ma, D., J. Tang, Q. Zhang, Z. Wei, F. Gao, and Z. Feng, "Integrated sensing and communications network design and key technologies for low-altitude economy," *China Communications*, Vol. 22, No. 9, 81–102, 2025.

[5] He, D., W. Yuan, J. Wu, and R. Liu, "Ubiquitous UAV communication enabled low-altitude economy: Applications, techniques, and 3GPP's efforts," *IEEE Network*, Vol. 40, No. 1, 115–122, Jan. 2026.

[6] Chen, Q., W. Guo, and L. Xu, "Research on the low-altitude airspace communication and surveillance system," in *Discovery, Innovation and Communication — 5th CSAA Science and Technique Youth Forum*, 714–717, Oct. 2012.

[7] Li, S., J. Tang, B. Zheng, L. Zhu, C. Yang, N. Zhao, X. Y. Zhang, and K.-K. Wong, "Rotatable antenna system empowered low-altitude economy: Opportunities and challenges," *IEEE Wireless Communications*, Vol. 33, No. 1, 116–123, 2026.

[8] Wei, M., Y. Zhao, and J. Yu, "Research on low altitude network coverage solutions," in *2025 International Wireless Communications and Mobile Computing (IWCMC)*, 412–417, Abu Dhabi, United Arab Emirates, 2025.

[9] Hong, W., "Solving the 5G mobile antenna puzzle: Assessing future directions for the 5G mobile antenna paradigm shift," *IEEE Microwave Magazine*, Vol. 18, No. 7, 86–102, Nov.–Dec. 2017.

[10] Tian, J., Y. Han, S. Jin, J. Zhang, and J. Wang, "Analytical channel modeling: From MIMO to extra large-scale MIMO," *Chinese*

Journal of Electronics, Vol. 34, No. 1, 1–15, 2025.

[11] Sun, R. R., W. Keusgen, and D. Viorel, "MIMO channel capacity measurements in an indoor-office environment at 6 and 37 GHz," in *2024 IEEE Globecom Workshops (GC Wkshps)*, 1–7, Cape Town, South Africa, 2024.

[12] Pozar, D. M. and S. M. Duffy, "A dual-band circularly polarized aperture-coupled stacked microstrip antenna for global positioning satellite," *IEEE Transactions on Antennas and Propagation*, Vol. 45, No. 11, 1618–1625, Nov. 1997.

[13] Liang, M. Y., X. Y. Li, X. T. Tian, H. B. Zhang, and H. H. Zhang, "Satellite communication smartphone circularly polarized antenna," in *2024 14th International Symposium on Antennas, Propagation and EM Theory (ISAPE)*, 1–2, Hefei, China, 2024.

[14] Ullah, S., Y. He, A. Majeed, and Y. Huang, "A low-profile wideband dual-sense circularly polarized MIMO antenna for mmWave applications," *IEEE Antennas and Wireless Propagation Letters*, Vol. 24, No. 8, 2163–2167, Aug. 2025.

[15] Xue, Y., C. Mao, L. Zhang, R. Tafazolli, and A. Kishk, "Broadband circularly polarized helical antenna decoupling for massive MIMO applications," *IEEE Antennas and Wireless Propagation Letters*, Vol. 24, No. 10, 3515–3519, 2025.

[16] Meng, Y., A. Ren, C. Wang, G. Xu, L. Zhao, Y. Li, L. Yang, and Z.-X. Huang, "Metasurface-loaded circularly polarized dual-band MIMO cellphone frame antenna for mobile communication applications," *IEEE Antennas and Wireless Propagation Letters*, Vol. 24, No. 8, 2168–2172, 2025.

[17] Ullah, S., Y. He, and Y. Huang, "A triband circular-polarized four-port MIMO antenna with compact size and low mutual coupling," *IEEE Antennas and Wireless Propagation Letters*, Vol. 24, No. 3, 621–625, Mar. 2025.

[18] Tiwari, R. N., V. Kaim, P. Singh, T. Khan, and B. K. Kanaujia, "Semi-flexible diversified circularly polarized millimeter-wave MIMO antenna for wearable biotechnologies," *IEEE Transactions on Antennas and Propagation*, Vol. 71, No. 5, 3968–3982, May 2023.

[19] Khan, A., Y. He, and Z. N. Chen, "A dual-band quad-port circularly polarized MIMO antenna based on a modified Jerusalem-cross absorber for wireless communication systems," *IEEE Transactions on Antennas and Propagation*, Vol. 72, No. 1, 310–322, Jan. 2024.

[20] Khan, A., Y. He, Z. He, and Z. N. Chen, "A compact quadruple-band circular polarized MIMO antenna with low mutual coupling," *IEEE Transactions on Circuits and Systems II: Express Briefs*, Vol. 70, No. 2, 501–505, Feb. 2023.

[21] Wen, Y., Z. Zhang, S.-W. Wong, C. Ji, R. Liu, and Y. He, "Low-RCS Metasurface-based Dual Circularly-Polarized MIMO Antenna with Polarization and Spatial Diversity," *IEEE Transactions on Instrumentation and Measurement*, Vol. 74, 1–10, 2025.

[22] Yang, W. J., Y. M. Pan, and S. Y. Zheng, "Design of self-decoupled circularly polarized MIMO dielectric resonator antenna arrays based on polarization orthogonality," *IEEE Transactions on Antennas and Propagation*, Vol. 72, No. 2, 1192–1200, Feb. 2024.

[23] Gupta, S. K. and A. Sharma, "Octa-port dual-polarized antenna/rectenna for MIMO simultaneous wireless information and power transfer (SWIPT)," *IEEE Microwave and Wireless Technology Letters*, Vol. 35, No. 1, 99–102, Jan. 2025.

[24] Hussain, N., M.-J. Jeong, A. Abbas, and N. Kim, "Metasurface-based single-layer wideband circularly polarized MIMO antenna for 5G millimeter-wave systems," *IEEE Access*, Vol. 8, 130 293–130 304, Jul. 2020.

[25] Ren, X., H. Zhai, Y. Jia, M. Wang, and Y. Lei, "Wideband RCS reduction for circular-polarized slot array antennas based on composite metasurface," *IEEE Antennas and Wireless Propagation Letters*, Vol. 23, No. 12, 4867–4871, Dec. 2024.

[26] Aghoutane, B., S. Das, M. E. Ghzaoui, B. T. P. Madhav, and H. E. Faylali, "A novel dual band high gain 4-port millimeter wave MIMO antenna array for 28/37 GHz 5G applications," *AEU — International Journal of Electronics and Communications*, Vol. 145, 154071, 2022.

[27] Kim-Thi, P. and T. T.-L. Nguyen, "Circularly polarized MIMO patch antenna with high isolation and wideband characteristics for WLAN applications," *Heliyon*, Vol. 9, No. 9, e19450, 2023.

[28] Jamal, M. Y., M. Li, and K. L. Yeung, "Isolation enhancement of closely packed dual circularly polarized MIMO antenna using hybrid technique," *IEEE Access*, Vol. 8, 11 241–11 247, Jan. 2020.

[29] Kumar, S., G. H. Lee, D. H. Kim, H. C. Choi, and K. W. Kim, "Dual circularly polarized planar four-port MIMO antenna with wide axial-ratio bandwidth," *Sensors*, Vol. 20, No. 19, 5610, 2020.

[30] Sufian, M. A., N. Hussain, A. Abbas, J. Lee, S. G. Park, and N. Kim, "Mutual coupling reduction of a circularly polarized MIMO antenna using parasitic elements and DGS for V2X communications," *IEEE Access*, Vol. 10, 56 388–56 400, May 2022.